

Atomistic study of energy funneling in the light-harvesting complex of green sulfur bacteria

Joonsuk Huh,^{1,*} Semion K. Saikin,¹ Jennifer C. Brookes,^{1,2}
Stéphanie Valteau,¹ Takatoshi Fujita,¹ and Alán Aspuru-Guzik^{1,†}

¹*Department of Chemistry and Chemical Biology,
Harvard University, Cambridge, Massachusetts 02138, United States*

²*Department of Physics and Astronomy, University College London, Gower, London WC1E 6BT*

Phototrophic organisms such as plants, photosynthetic bacteria and algae use microscopic complexes of pigment molecules to absorb sunlight. Within the light-harvesting complexes, which frequently have multiple functional and structural subunits, the energy is transferred in the form of molecular excitations with very high efficiency. Green sulfur bacteria are considered to be amongst the most efficient light-harvesting organisms. Despite multiple experimental and theoretical studies of these bacteria the physical origin of the efficient and robust energy transfer in their light-harvesting complexes is not well understood. To study excitation dynamics at the systems level we introduce an atomistic model that mimic a complete light-harvesting apparatus of green sulfur bacteria. The model contains about 4000 pigment molecules and comprises a double wall roll for the chlorosome, a baseplate and six Fenna-Matthews-Olson trimer complexes. We show that the fast relaxation within functional subunits combined with the transfer between collective excited states of pigments can result in robust energy funneling that is weakly dependent on the initial excitation conditions and temperature changes. Moreover, the same mechanism describes the coexistence of multiple timescales of excitation dynamics frequently observed in ultrafast optical experiments. While our findings support the hypothesis of supertransfer, the model reveals energy transport through multiple channels on different length scales.

I. INTRODUCTION

Photosynthetic bacteria are among the simplest organisms on Earth which use sunlight as their main energy source [1]. To collect solar energy these bacteria exploit light-harvesting complexes (LHC), aggregates of pigment molecules, which collect photons and transfer the associated energy at the submicron scale. The LHC in green sulfur bacteria contains large light absorbing antennae self-assembled in the so-called chlorosome [2]. These bacteria are obligate phototrophs – they are required to use sunlight to support metabolic reactions [3–5]. However, it has been observed that green sulfur bacteria can live in extremely low light conditions, even when receiving only a few hundred photons *per bacterium* per second [6–8]. These facts have inspired many conjectures and discussions on the functional properties, energy conversion efficiency and robustness of LHC in green sulfur bacteria [9–14].

In order to address this controversy we introduce a model which includes atomistic structural detail of the green bacteria LHC and allows for the simulation of excitation energy transfer (EET) at the systems level. As a specific example, we consider the LHC of *Chlorobium tepidum*. We observe fast relaxation of excitations within the subunits of LHC owing to the large overlap between exciton states and strong interaction with environmental fluctuations. The transfer between subunits involves collective excited states of the pigment

molecules and supports the hypothesis of supertransfer [12–14]. The energy transport is robust to different initial excitation conditions, and changes in temperature. Finally, we show that the population of different parts of the LHC can be described using simple kinetic equations with time-dependent transfer rates characterizing intra-unit dynamics. This later model naturally explains the multiple timescales of EET reported in optical studies of green sulfur bacteria [15–19] and green non-sulfur bacteria [20–22].

Theoretical models have been applied mostly to single functional units of LHCs [23–31] in order to understand the physical principles of energy transfer. Some of these studies also involved atomistic structures [29, 31–33], which make the models computationally demanding. To the authors knowledge there are only a few atomistic studies of the complete light-harvesting systems of purple bacteria [34, 35] but none for green sulfur bacteria. In addition to the large scale calculations the detailed analysis of excitation dynamics on the systems level [22, 34–37] is complicated due to the lack of structural information. Thus, one usually needs to use macroscopic phenomenological models [38] or introduce additional constraints and approximations on the transport models [39, 40]. Our work is, as mentioned already, the fully atomistic picture from chlorosome to cytoplasm of green photosynthetic bacteria.

The LHC in green sulfur bacteria is composed of bacteriochlorophyll (BChl) pigment molecules. These monomers aggregate in several interconnected functional units, as shown in Fig. 1A. The main element of LHC is the chlorosome - an ellipsoidal shaped body of size ranging from tens to hundreds of nanometers [2]. The

* Email: huh@fas.harvard.edu

† Email: aspuru@chemistry.harvard.edu

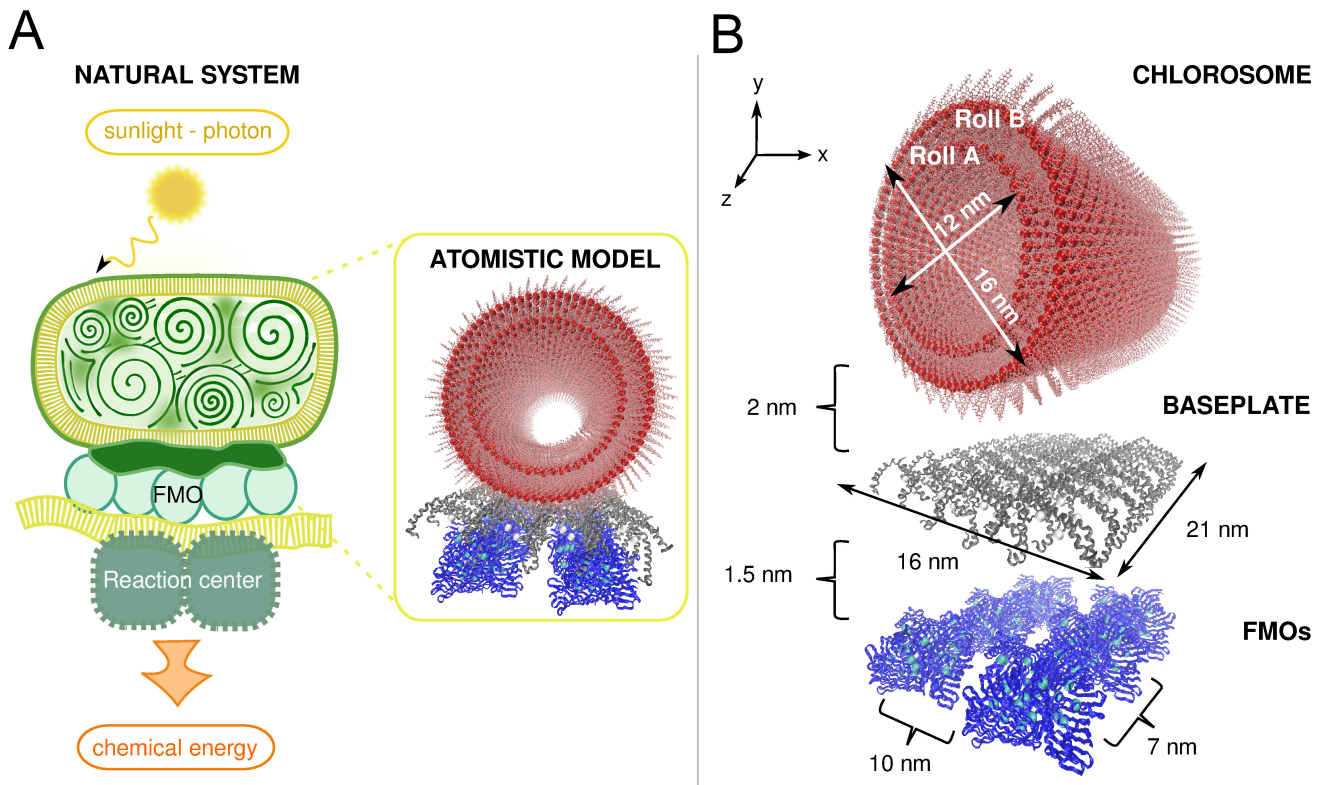


FIG. 1. **Photosynthetic apparatus.** **A**, Cartoon of light-harvesting complex in green sulfur bacteria. The bacteria transform solar photons into chemical energy. Sunlight absorbed by the chlorosome is transferred in the form of an exciton through the baseplate and Fenna-Matthews-Olson (FMO) complexes subsequently to the reaction center. The electro-chemical potential energy gradient is generated over a membrane and the energy is transformed as chemical energies finally. A snapshot of the model structure is also shown. **B**, Atomistic model with corresponding length scales. The atomistic model is composed of a double wall roll for the chlorosome (Roll A: 1620 ($=60 \times 27$) BChl *c* sites and Roll B: 2160 ($=80 \times 27$) BChl *c* sites), baseplate (64 BChl *a* sites) and 6 FMO trimer complexes (144 ($=24 \times 6$) BChl *a* sites).

chlorosome is densely packed with BChl *c* pigments. Two other functional units - the baseplate [41] and the Fenna-Matthews-Olson (FMO) trimer complex [42] are composed of BChl *a* pigments held together by a protein scaffolding. Energy in the form of molecular excitations (*i.e.* exciton) is collected by the chlorosome and funneled through these antenna units to the reaction center where charge carriers are then generated.

At low light intensities only the lowest electronic excitations of BChls, Q_y transitions are involved in energy funneling. The distance between the pigments in LHCs is sufficiently large such that the overlap of electronic wave functions are assumed to be negligible. In this case the energy transfer is mediated by the near field interaction between molecular electronic transitions, the Förster interaction [43–45]. If the interaction between several molecules is sufficiently strong as compared to the energy difference between their electronic transitions, the exciton states are delocalized over the group of pigments [44, 45]. The preferential direction for energy transport is controlled by the frequencies of electronic transitions: the excitation goes to molecules or group of molecules with lower excited state energy, while dissipat-

ing the energy difference to the environment.

A. Molecular aggregate model

A single LHC of *Chlorobium tepidum* contains 200–250 thousand BChl molecules [2, 18, 46]. Most of these molecules are found in the chlorosome. The model we have created is shown in Fig. 1, it contains 3988 pigments and represents all the functional units of LHC in green sulfur bacteria, excluding the reaction center.

In our model (Fig. 1B) a double wall roll aggregate with diameter of about 16 nm and length of about 21 nm, represents the chlorosome. Several possible structural arrangements of BChls in the chlorosome have been investigated theoretically and experimentally [47]. Here we use the structure of Ref. [48], obtained from a triple mutant bacteria and characterized with nuclear magnetic resonance and cryo-electron microscopy. This structure is also supported by 2-dimensional polarization fluorescence microscopy experiments [49].

The microscopic structure of the baseplate has not yet been experimentally verified [41]. We construct a base-

plate lattice as following. The unit cell consists of dimers of CsmA proteins [50] containing 2 BChl *a* molecules sandwiched between the hydrophobic regions and bound near the histidine. To establish a stable structure of the baseplate, classical molecular dynamics simulations were done using the NAMD program package version 2.8 [51]. Force fields were parameterized with a combination of Amber ff99SB for the protein [52] and MMFF94 atomic charges for the BChl *a*. The final structure complies with the periodicity and dimensions of the unit cell as seen in freeze frame fracture [53]. Moreover, the circular dichroism and fluorescence anisotropy spectra of the constructed baseplate agree with the measured spectra [21, 50]. Finally, for the FMO protein complexes we employ the structure resolved in Ref. [54].

The constructed model of the light-harvesting apparatus, shown in Fig. 1B, contains 95 % of BChl *c* and 5 % of BChl *a*, which is comparable to the stoichiometry of the natural system (99 % and 1 %) [18]. The estimated density of FMO complexes is about 1 FMO/50 nm² [55]. Therefore, we distribute 6 FMO complexes under the baseplate which occupies about 300 nm² (see Fig. 1B). This gives a pigment ratio of 2.3:1 (FMOs:baseplate), which is similar to the corresponding stoichiometry of *Chlorobium tepidum* 2:1 [46]. The distances between the chlorosome BChl *c* aggregates and the baseplate is determined by the length of BChl *c* esterifying alcohols. In the case of *Chlorobium tepidum* it is about 2 nanometers [19, 22, 41]. While the orientation of FMO relative to the baseplate has been verified experimentally [55], the relative distance between these units is unknown. In our model we set it to be 1.5 nm, which is larger than the inter-pigment distance within FMO but smaller than the baseplate-chlorosome distance. This choice is based on the argument that the FMO complex is strongly linked to the baseplate [56]. Minor variations of this distance do not affect the results.

The frequencies of exciton transitions in LHCs are controlled by multiple factors. In the model it is equivalent to use the relative shifts (energy gap) of these transitions, which are relevant to the EET provided that no exciton annihilation is involved. These shifts can be calculated from the pigment-pigment couplings and the electronic excitations of single BChls, site energies, modified by the local environment [57]. While the couplings can straightforwardly be computed using a screened dipole-dipole model [57], the calculation of site energies requires more complicated models or fitting to experimentally measured optical spectra.

Here, we set the frequency offset to be aligned with the lowest site energy of the FMO complex [56, 58]. The absorption domains of the baseplate and FMO composed of BChl *a* pigments are not clearly distinguishable. The absorption band of the baseplate covers the range 790–810 nm. This range also includes the absorption band of the FMO complexes [19, 58, 59]. In fact, the absorption band of the baseplate significantly overlaps with that of the chlorosome [19]. In order to reproduce these spec-

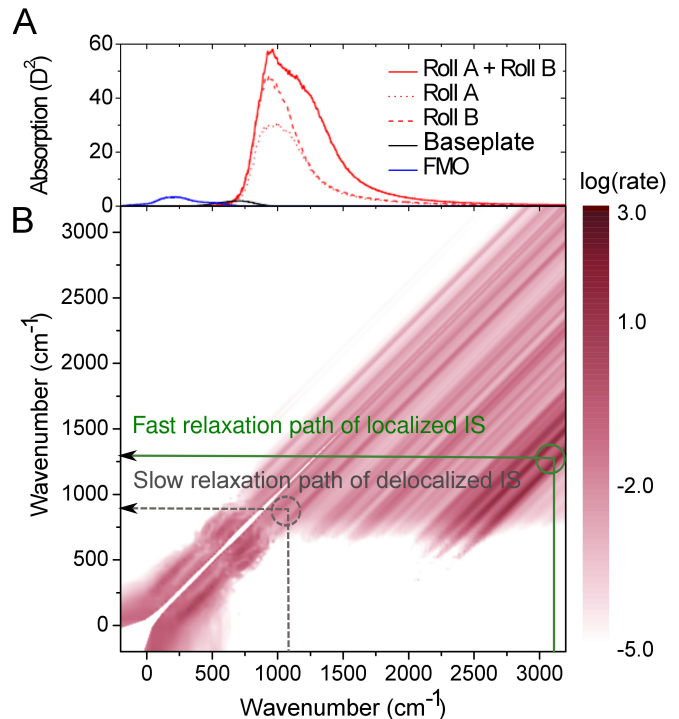


FIG. 2. **Calculated absorption spectra and exciton transfer rate matrix γ_{MN} .** **A**, Calculated absorption spectra [60] of the antenna units in Fig. 2 are shown. The absorption spectra are calculated and drawn for the double wall roll (Roll A + Roll B), the single rolls (Roll A and Roll B), the baseplate and the 6 FMO complexes. **B**, Exciton population transfer rate matrix γ_{MN} (cm⁻¹) at 300K is presented in a logarithmic scale. γ_{MN} indicates population transfer rate between exciton states $|M\rangle$ and $|N\rangle$. We set, here, the frequency offset to be aligned with the lowest site energy of the FMO complex.

tra using the constructed model we define the site energy of BChl *c* to be 3050 cm⁻¹, which places the absorption maximum of the chlorosome of about 740 nm above the absorption maximum of FMO complexes (see Fig. 2A). As a result, the corresponding absorption maxima of BChl *a* and *c* domains are found at 804 nm and 758 nm, respectively, when we use 12225 cm⁻¹ (818 nm) as the offset energy value.

B. Exciton transfer model

We describe the exciton dynamics with the Redfield quantum master equation, which includes coherent, dephasing and relaxation processes [57, 61–64]. The validity of the Redfield method for the EET in natural light-harvesting structures had been discussed by many authors, see *e.g.* Refs. [65–70] and the references cited therein. Yang and Fleming [67] claimed, for example, that the validity of the Redfield equation relies on the frequency domain of the phonon spectral density rather than the relatively weak exciton-phonon cou-

pling strengths with respect to the pigment-pigment couplings. When the energy gap between the exciton states is small, a broad spectral density can guarantee that the Redfield equation works well. Our molecular aggregate model in Fig. 1 and the corresponding spectral densities [29, 71] satisfy this condition: the absorption spectra of the antenna units overlap each other significantly. Novoderezhkin and *et al.* [68] proposed to compensate the underestimation of the transfer rate between exciton states with large energy gaps by increasing the spectral density in the high frequency region. Therefore, we note here the exciton transition rate, which involves the exciton transfer with a large energy gap, could be underestimated because the Redfield model can only account for the single phonon process. The multiphonon process could occur in the internal exciton dynamics of the antenna units due to its broad exciton bands (see Fig. 2A). The internal exciton dynamics of the chlorosome is, however, much faster than the exciton transfer between the antenna units. Thus, the Redfield model should give a reasonable results (timescales) qualitatively for the exciton funneling process of the photosynthetic apparatus. For more accurate models, one would consider other methods such as the modified Redfield approach [65, 67, 69], hierarchical equations of motion [27, 72–74], iterative linearized density matrix dynamics [75], non-Markovian quantum state diffusion [28, 76], variational master equation [77], path integral Monte Carlo [78], and see the references cited in the review [79] of the methodologies in EET. However, most of these sophisticated methods, are not applicable to our large system because they are numerically demanding.

In our model, the system-bath Hamiltonian of the light-harvesting apparatus is composed of three parts: the system consists of the local excitations of bacteriochlorophylls (BChls) and the point dipole interactions between them, described using a tight-binding Hamiltonian. Then, the system (BChls) is coupled linearly to the bath (proteins and solvent). The bath Hamiltonian consists of an infinite sum of multidimensional quantum harmonic oscillators (see *e.g.* Ref. [64]).

Within the secular approximation and in the Markov limit, the equations of motion of the reduced density operator $\hat{\rho}_S(t)$ in the exciton basis (*cf.* Ref. [80]) is written in a generalized Lindblad quantum master equation form [62, 81]. The population and coherence transfer can be decoupled within the secular approximation [70]. After ignoring pure dephasing terms (see *e.g.* Ref. [30] for the discussion) and degeneracy of the exciton states (numerical degeneracy within 1 cm^{-1}) [61], the final quantum master equation is given in a standard Lindblad form [62].

The resulting quantum master equation includes a term γ_{MN} , which is the exciton transition rate between the corresponding exciton states $|M\rangle$ and $|N\rangle$. γ_{MN} is calculated with the exciton eigenvectors and spectral density at the transition energy (see Ref. [64, 82] for the definition). It is shown in Fig. 2B as a matrix, for

the EET dynamics at 300 K. We unravel the standard Lindblad equation into a stochastic Schrödinger equation for numerical efficiency and propagate the stochastic wave functions with enough trajectories to converge to the master equation solution after the ensemble average \mathcal{E} [62].

A non-linear unraveling of the Lindblad equation is used for norm conservation of the wave function [62]. The non-linear stochastic Schrödinger equation is integrated with an exponential time integrator with time step 1 fs [83]. All results are obtained from 1000 ensemble averages, unless otherwise mentioned. We incorporate the effects of slow fluctuations in the site energies (static disorder). We use 100 cm^{-1} for the Gaussian fluctuations in FMO and the baseplate, and 500 cm^{-1} for the roll [58, 71].

The system Hamiltonian of FMO trimer complexes is taken from Ref. [56]. The spectral density from our previous work [29] is used: where molecular dynamics and time-dependent density functional theory calculations were used for obtaining it. A harmonic prefactor was used for the spectral density [82]. The structure of the double wall roll is obtained based on Ref. [48]. The structure was optimized with molecular dynamics simulation and a spectral density was obtained by time-dependent density functional theory calculations [71, 82].

Instead of computing the spectral density of the baseplate, which is composed of BChl *a*, it is obtained by scaling the spectral density of FMO [29]. This approximation is justified because we expect the vibrational structure to be similar to FMO's, which is surrounded by a protein environment (*cf.* chlorosome) and is also composed of BChl *a*. However, we expect a larger reorganization energy for the baseplate because the Stokes shift of the baseplate is about 300 cm^{-1} [19] while the Stokes shift of the FMO trimer complex is small [84].

To this end, we define the mean exciton energy to quantify the exciton energy dissipation from the system to the bath during the energy funneling process,

$$\text{MEE}(t) = \mathcal{E} \left(\text{Tr}_S \left(\hat{H}_S \hat{\rho}_S(t) \right) \right), \quad (1)$$

where \hat{H}_S is the system Hamiltonian and Tr_S is the trace over the system degrees of freedom.

Additionally, we introduce the cooperativity, which is used later to quantify the enhancement of transition dipole moment by coherence. Cooperativity(t) can be interpreted as excitation delocalization, as following

$$\text{Cooperativity}(t) = \frac{1}{|\mu|^2} \mathcal{E} \left(\left| \sum_{\alpha=x,y,z} \text{Tr}_S (\hat{\mu}_\alpha \hat{\rho}_S(t)) \right|^2 \right), \quad (2)$$

where $\hat{\mu}_\alpha$ is the transition dipole moment operator and a normalization factor $|\mu|^2 = 30 \text{ D}^2$, which is the absolute square of the transition dipole moment of a single pigment, is used. All pigments have the same magnitude of the transition dipole moment in our model (Fig. 1B).

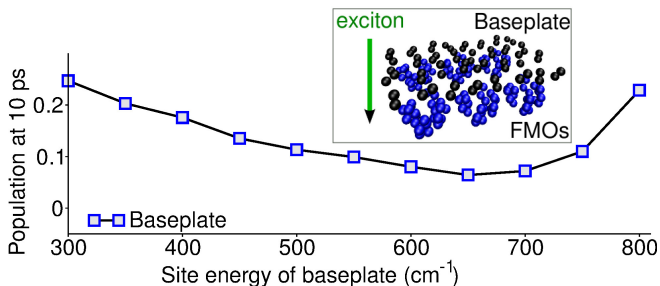


FIG. 3. **Scanning of the site energy of baseplate.** The remaining exciton population of the baseplate at 10 ps for the exciton relaxation from the baseplate to FMOs with varying site energies of the baseplate and using 500 ensemble average. A localized initial state at a single site in the middle of the baseplate is used for the exciton population dynamics.

II. EXCITATION ENERGY FUNNELING

To assign a site energy for the baseplate with the model structure described in the previous section, we scan over possible site energies of the baseplate ranging from 300 cm^{-1} to 800 cm^{-1} and calculate the resulting exciton dynamics including only the baseplate and FMO complexes. In Fig. 3 we show the remaining population on the baseplate at 10 ps, as a function of chosen site energies for the baseplate.

We propagate the quantum dynamics using scaling factors of 1, 2 and 3 to get the spectral density of the baseplate from that of FMO. As the scaling factor increases reorganization energy increases. Also, the site energy of the baseplate at the population minimum increases, because stronger exciton-phonon couplings make fast energy relaxation possible with small spectral overlap (see Fig. 2A), and prevents population from getting trapped in the baseplate. The differences, however, are not large among the results of the scaling factors and thus the exciton dynamics is robust respect to the choice of the scaling factor. Fig. 3 shows the results using scaling factor 2. The remaining exciton populations on the roll at 10 ps are in 10–20% over the site energy range. We choose 650 cm^{-1} as a site energy of the baseplate. This corresponds to the case where the population is smallest at 10 ps in Fig. 3. The resulting absorption spectrum of the baseplate is shown in Fig. 2A.

To fully characterize the EET dynamics of the photosynthetic apparatus model in Fig. 1, one needs to study the exciton dynamics for all possible initial (exciton) states within an ensemble at a finite temperature. For instance, the initial state prepared by a coherent light source (laser) could be considered as a single exciton state [85]. Instead of studying all possible initial exciton states, we perform exciton dynamics simulations for two different cases of initial excitation at 300 K to see how the initial condition affects the EET dynamics. One is the brightest exciton state of the system Hamiltonian of Roll A, which is delocalized over Roll A (see the snap-

shot of Fig. 4A at 0 ps) and has energy 1078 cm^{-1} . The other initial condition to be considered is a localized initial state (IS). In particular, a single site located on top and in the middle of Roll A is selected for the localized IS having energy 3126 cm^{-1} (see the snapshot of Fig. 4B at 0 ps).

Comparing the absorption spectra of Roll A and Roll B in Fig. 2A, one can see the peak maximum of Roll B is red-shifted from the peak maximum of Roll A, thus there is an exciton energy gradient between the layers. As the radius of the roll increases (contrast A and B), the peak maximum shifts to the red [20, 47, 60]. This occurs because the roll curvature changes and this induces stronger dipole-dipole interactions between neighboring pigments. This energy gradient is favored by the exciton energy funneling because EET from the outermost layer to the baseplate is important. Our choice of the initial states on the Roll A is based on this argument.

There are two important factors in determining the exciton transfer between the antenna units. These are the energy resonance condition and the excitonic coupling between the energy levels of the antenna units [86]. The former is the necessary condition for the EET between the units and the later determines how fast EET should be. Fig. 2 shows the delocalized IS is close to the energy levels of the baseplate and large multichromophoric excitonic coupling strengths to the baseplate exciton states, while the localized IS is far from the energy resonance level to the baseplate and the excitonic coupling strength is small.

Fig. 4 summarizes the resulting exciton dynamics at 300 K. Figs. 4A and 4B show the population dynamics using the delocalized IS and the localized IS respectively and up to 10 ps. Our choice of the time interval (10 ps) of the EET simulation is based on the timescales of the EET of *Chlorobium tepidum* in Ref. [19]. Snapshots of the site populations at 0 ps, 0.1 ps and 10 ps are shown below the population plots. The exciton population distributions of individual antenna units at 10 ps are almost identical regardless of the initial conditions, for example, the total exciton population on FMOs using the delocalized IS is 66% of the initial population, which is only 2% higher than that using the localized IS.

A. Short time dynamics

The EET dynamics of the delocalized IS and the localized IS become similar within 1 ps (Fig. 4). The short time dynamics ($< 200\text{ fs}$), however, are different. Fig. 4A shows a fast initial population decay for the roll comparing to that of the localized IS in Fig. 4B. Characteristic time constants in Table I for the dynamics are extracted by three-exponential fitting of the exciton populations of the roll such that amplitudes are summed to be 100%. By comparing the time constants for the roll in Table I, we see that Set I (Fig. 4A) has a fast sub-100-fs component while Set III (Fig. 4B) does not. However, τ_1 in

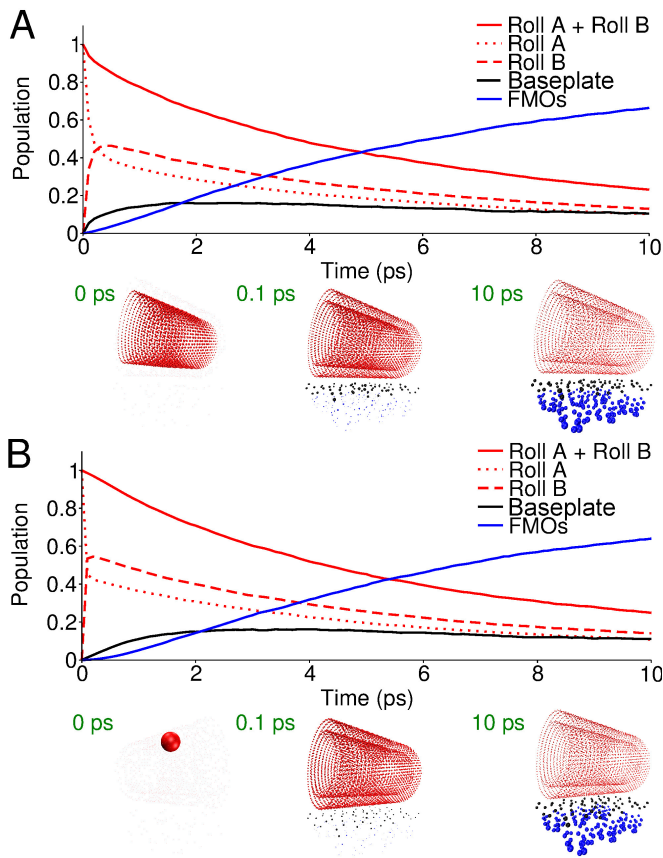


FIG. 4. **Exciton population dynamics with a delocalized and a localized initial state at 300 K.** **A**, The initial state (see the snapshot at 0 ps) is the brightest state of Roll A. **B**, The initial state (see the snapshot at 0 ps) is a localized state, *i.e.* a site on the top and in the middle of the Roll A. The locations of magnesium (Mg) in the BChls represent the locations of exciton sites and the sizes of the spheres are proportional to the populations of the corresponding sites. The populations of the rolls, the baseplate and the FMOs are designated red, black and blue, respectively.

Set I accounts for only 6% of the 10 ps exciton dynamics. In the case of using the delocalized IS, the single exciton starts to migrate from the roll to the baseplate already at the very beginning (< 100 fs). This occurs because energetically, the brightest exciton state, *i.e.* the delocalized IS (1078 cm^{-1}) is close to the baseplate absorption region (see Fig. 2A) and has a large collective transition dipole moment. On the other hand, the localized IS of a single site (3126 cm^{-1}) is far from the energy resonant region and has a comparably weak transition dipole moment. Complete equilibration is achieved within 100 fs for the localized IS dynamics and almost no exciton population is transferred to the baseplate in this short time. This can be seen in the inset figure of Fig. 5.

The inset figure of Fig. 5 shows the diffusion process in the roll with the localized IS for the first 200 fs. Snapshots of the roll populations at 0, 10 and 20 fs are placed above the inset plot. In this plot, one can see how the sin-

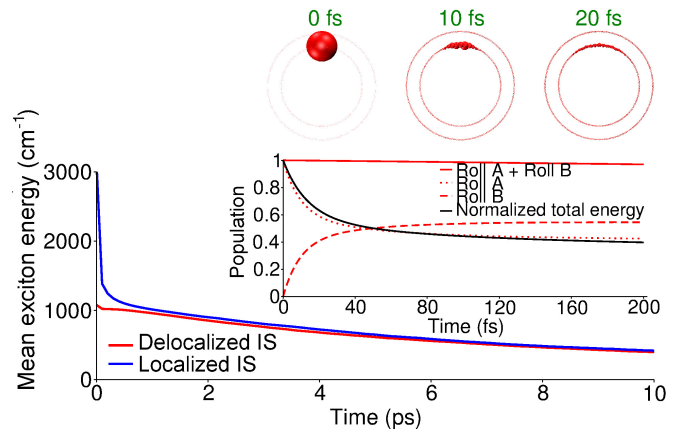


FIG. 5. **Mean exciton energy with a delocalized and a localized initial state at 300 K.** Mean exciton energy (Eq. 1) with the two different initial excitations, which correspond to those in Fig. 4A and 4B. The short time dynamics for the first 200 fs of Fig. 4B is given in the inset figure with the corresponding population snapshots. The populations in the snapshot which are projected to the long axis of the rolls. The locations of magnesium (Mg) atoms in the BChls represent the locations of exciton sites and the sizes of the spheres are proportional to the populations of the corresponding sites.

gle exciton diffuses within and between the layers. The black solid line in the inset figure is the mean exciton energy (Eq. 1), which is normalized to the initial energy (3126 cm^{-1}). Interestingly, the curve is similar to the population dynamics of Roll A. From this we can conclude that the population transfer from Roll A to Roll B is the main energy relaxation channel and the slight difference of the two curves indicates the effect of population redistribution within the single layers. Thus the energy dissipation due to exciton-phonon coupling mainly causes exciton transfer between the layers in this initial short time period. The mean exciton energy of the total system (Roll+baseplate+FMOs) is given in Fig. 5 for two different initial excitations. The solid blue line and the solid red line correspond to the exciton dynamics of Fig. 4A and Fig. 4B, respectively.

As mentioned above, the initial energy of the delocalized state is already close to the baseplate bright state energy domain (see Fig. 2), while that of the localized state is higher (3126 cm^{-1}). In the localized IS case, the excess energy (about 2000 cm^{-1}) relative to the delocalized IS should be released to the environment in order for resonant energy transfer to the baseplate to occur. In spite of the high initial energy of the localized IS, which is far from the energy resonance domain, the exciton population of each unit at 10 ps is similar to that of the delocalized IS case (see Fig. 4A). This is possible because a rapid energy relaxation channel (Fig. 2B) is available for the dynamics of Fig. 4B. The blue line in Fig. 5 shows a rapid energy drop within 100 fs. Then, within 1 ps, the total energy approaches the energy of the delocalized IS. The population snapshots at 100 fs indicate that popula-

tion distributions are quite similar. Also, the population on the roll in Fig. 4B at that time indicates that, by 100 fs, the system population is mostly distributed over delocalized states. The mean exciton energy obtained from the exciton dynamics with the delocalized IS and the localized IS become similar within 500 fs. The rapid relaxation within the roll results in robust energy transfer from the roll to the FMOs in the long time limit.

Microscopically, the energy dissipation dynamics is determined by thermal excitations and relaxation among exciton levels. The energy dissipation rate, in this model, depends on the spectral density, a quantity which indicates how strongly exciton states are coupled to the thermal bath, the probability distribution of the exciton states and temperature.

In Fig. 2B, we show the exciton transfer matrix (γ_{MN}) at 300 K in logarithmic scale ($\log(\text{cm}^{-1})$). We indicate the fast energy dissipation path for the localized IS with a green arrow. The strong red diagonal band corresponds to the strong exciton-phonon coupling at 1600–2000 cm^{-1} [87], which leads to the rapid energy dissipation in the localized IS. Damjanović *et al.* [32] suggested that a weakly bound polaron can be formed in BChl aggregates due to the interaction of excitons with intramolecular vibrational mode at about 1670 cm^{-1} . Their results were based on studies of LHC in purple bacteria. We do expect that the polaron couplings can renormalize energy levels and the mobility of the exciton energy is reduced [32]. This should be, however, weaker in the chlorosome where BChls are densely packed and the pigment-pigment interaction is, accordingly, stronger than that of LHC in purple bacteria.

The population dynamics of the FMOs depends mainly on the population of the baseplate because direct population transfer from the roll to FMOs is negligible (see Set IV in Table I). Therefore, the short time dynamics of FMOs are different from each other in Figs. 4A and 4B. Exciton populations of FMOs increase linearly and parabolically in the short time, respectively, in Figs. 4A and 4B. However, after 3 ps, the population dynamics converge to each other.

B. Cooperativity of the excitonic states

In multichromophoric systems, coherence between donor molecules can lead to a large collective transition dipole moment which contributes to enhancing the energy transfer from the donor to acceptor groups as compared to incoherent hopping between individual molecules [12–14, 88].

In Fig. 6, we show the cooperativity of Roll A only (excluding Roll B, the baseplate and FMOs) for 500 fs. The cooperativity is calculated for three different initial excitation conditions: i) a delocalized IS for the brightest state of Roll A (blue), ii) a localized IS on a single site on top and in the middle of Roll A (red) and lastly iii) a delocalized IS on a single ring in the middle which has an equal amplitude and phase over the ring (black).

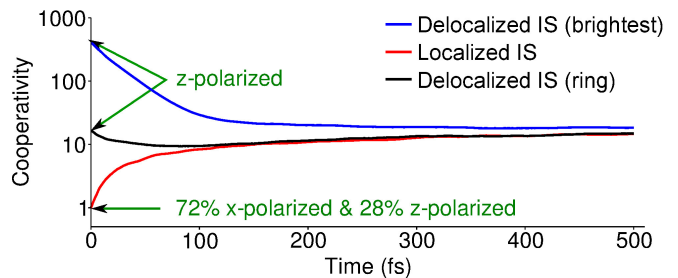


FIG. 6. **Time dependent cooperativity of Roll A only (without Roll B, the baseplate and FMOs) at 300 K.** The cooperativity (Eq. 2), dimensionless normalized collective transition dipole moment, is given in logarithmic scale. Three initial states are tested i) a delocalized IS for the brightest state of Roll A (blue), ii) a localized IS on a single site on top and in the middle of Roll A (red) and lastly iii) a delocalized IS on a single ring in the middle which has an equal amplitude and phase over the ring (black).

an equal amplitude and phase over the ring (black).

The delocalized IS (brightest) is z-polarized (along the length of the roll) and initially has a cooperativity of 402. This strong collective oscillator strength can induce rapid supertransfer [12–14] along the z-direction. The delocalized IS (ring) is also z-polarized because the selected initial state has the equal phase over all components. The initial cooperativity of the delocalized IS (ring) is 16. The localized IS has an initial cooperativity value of unity, which is 72% x- and 28% z-polarized. This difference in cooperativity at varying initial condition is one of the reasons why a fast decay component is found for the delocalized IS case only. However, the cooperativity of the delocalized IS drops quickly within 500 fs.

Regardless of the initial conditions, within 500 fs, all cooperativity values converge to a similar value (~ 15), which is still larger than 1, and the effective transition dipole moment becomes about 30% x-, 30% y- and 40%

TABLE I. **Time constants of the exciton dynamics of the chlorosome roll.** The values are obtained by three-exponential fittings ($A_1 \exp(-t/\tau_1) + A_2 \exp(-t/\tau_2) + A_3 \exp(-t/\tau_3)$) of the exciton population dynamics for each antenna unit. The amplitudes (A_1 , A_2 and A_3) are summed to be 100%.

Set	τ_1 (fs)	$(A_1(\%))$	τ_2 (ps)	$(A_2(\%))$	τ_3 (ps)	$(A_3(\%))$
I ^a	91.2	(6)	1.9	(22)	8.7	(72)
II ^b	109.4	(8)	2.4	(26)	9.5	(66)
III ^c	-	-	3.7	(57)	13.9	(43)
IV ^d	-	-	10.7	(5)	1500.0	(95)
Ref. [19] ^e	-	-	1.1	(42)	12.1	(58)

^a Corresponds to the exciton dynamics of Fig. 4A

^b Brightest delocalized initial state of Roll B is used.

^c Corresponds to the exciton dynamics of Fig. 4B

^d The baseplate is not included in the exciton dynamics.

^e Anisotropic decay of *Chlorobium tepidum* at 807 nm

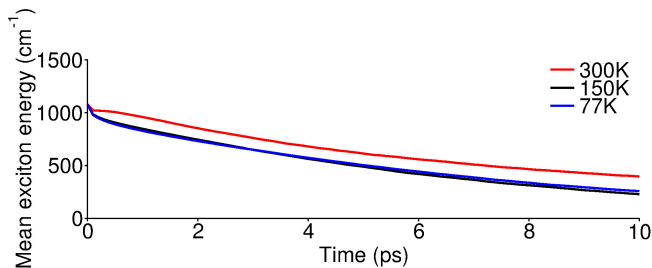


FIG. 7. **Temperature dependence of the mean exciton energy.** The mean exciton energy of the system (Eq. 1) is plotted at 300 K, 150 K and 77 K. The delocalized exciton initial state in Fig. 4A is used.

z-polarized. This is a favorable situation, in our photosynthetic apparatus model, as y-polarization (normal direction to the baseplate) is useful to funnel energy towards the baseplate. These results may indicate a multichromophoric effect [86]; *i.e.* the effective dipole moment of the delocalized exciton state is enhanced by symmetry, thus the exciton transfer coupling strength of exciton states of roll and the baseplate becomes large enough for rapid transfer even though the chromophores are far apart (> 2.0 nm) (see also Ref. [89] for the discussion on the coherence and EET rate).

C. Temperature dependence of the energy funneling

In the previous subsections, we showed that the exciton energy funneling process is robust to variations in initial excitation conditions due to the fast internal exciton dynamics of the roll. We now investigate the temperature effect by simulating the exciton population dynamics with the delocalized IS initial condition, *i.e.* the brightest state of Roll A, at 150 K and 77 K in Fig. 7.

The mean exciton energy curve at room temperature (300 K) in Fig. 4A is only slightly different from the curves at 150 K and 77 K in Fig. 7. This indicates that exciton transfer is robust within this temperature range. The robust energy transfer within the temperature range is due to the fast internal exciton dynamics of roll. The thermal excitation within the temperature range does not lift the exciton levels far from the energy resonance domain between the roll and the baseplate.

Thermal excitation in the temperature range (77, 150 and 300 K) can provide various channels towards the neighboring exciton states for the relaxation process (see Fig. 2B). Thermal excitation can also induce back transfer from the baseplate to the rolls [88] but it reduces the possibility of being trapped in dark states.

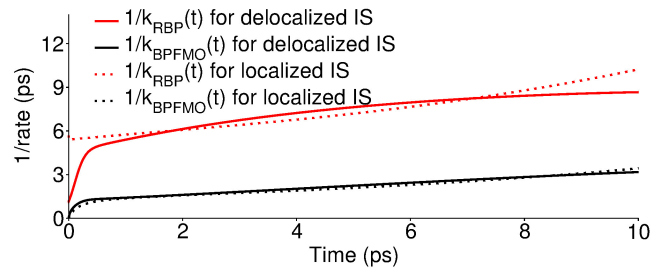


FIG. 8. **Time dependent reciprocal rate.** Time-dependent exciton transfer rates are given as the corresponding time constants, the reciprocal rate, for the exciton dynamics of the delocalized IS and the localized IS in Fig. 4. $k_{\text{RBP}}(t)$: exciton transfer rate from the roll to the baseplate. $k_{\text{BPFMO}}(t)$: exciton transfer rate from the baseplate to the FMOs.

D. Population kinetics

So far, we have shown that regardless of initial conditions and temperature about 70% of the exciton can be transferred to the FMOs within 10 ps. This robustness to the choice of initial conditions implies that internal dynamics within the roll is faster than energy transfer between the antenna units. We now proceed to examine the population dynamics by using a simple first order kinetic model (more sophisticated kinetic models in the EET of the LH complex networks can be found in *e.g.* Refs. [39, 40, 90, 91]):

$$\frac{d}{dt} \begin{pmatrix} [R](t) \\ [BP](t) \\ [FMO](t) \end{pmatrix} = \begin{pmatrix} -k_{\text{RBP}}(t) & 0 & 0 \\ k_{\text{RBP}}(t) & -k_{\text{BPFMO}}(t) & 0 \\ 0 & k_{\text{BPFMO}}(t) & 0 \end{pmatrix} \begin{pmatrix} [R](t) \\ [BP](t) \\ [FMO](t) \end{pmatrix} \quad (3)$$

where $[\cdot](t)$ denotes the population of each antenna unit, and $[R]$ and $[BP]$ are the population of the full roll (Roll A + Roll B) and the baseplate respectively. $k_{\text{RBP}}(t)$ is the exciton transfer rate from the roll to the baseplate and $k_{\text{BPFMO}}(t)$ is the one from the baseplate to the FMOs. The population transfer between the antenna units is characterized by time-dependent rate constants $k(t)$. Note that the internal dynamics within the antenna units, such as relaxation and thermal excitation among the exciton states, can be incorporated into the time dependence of $k(t)$. $k(t)$ physically corresponds to the multichromophoric Förster resonance energy transfer rate [86], because it quantifies energy transfer between the donor group (exciton states) of the roll and the acceptor group of the baseplate. The enhancement of energy transfer due to coherence (Fig. 6) between donor molecules is also referred as to supertransfer [12–14].

To test if there is direct exciton transfer from the roll to the FMO, we simulate the exciton dynamics without the baseplate in the energy funneling process. Set IV in Table I shows the result, the population dynamics of the roll is composed of 10 ps and 1.5 ns timescales with 5% and 95% amplitudes respectively. Thus, the exciton trans-

fer from the roll to FMOs is extremely slow such that only 3% is transferred within 10 ps. The direct exciton transfer from the roll to the FMO complexes is virtually negligible within the time interval of the EET dynamics 10 ps. In this kinetic model, thus, we assume there is no population transfer from low to high energy units and no direct transfer from the roll to FMOs (see Set IV in Table I).

The exciton populations in Fig. 4 are fitted to the kinetic model using least squares. The resulting time-dependent population transfer rates are shown in Fig. 8 for the exciton dynamics of Fig. 4, using both initial conditions (the delocalized IS and the localized IS). The initial and final values of the reciprocal rates of the (chlorosome) roll $1/k_{\text{RBP}}(t)$ have similar values to τ_2 and τ_3 of Sets I and III in Table I. Within 500 fs, $k_{\text{RBP}}(t)$ for the delocalized IS drops rapidly to a slower rate, with a similar timescale to the equilibrium time of the cooperativity (Eq. 2), see solid blue line in Fig. 6. However we see that $k_{\text{RBP}}(t)$ for the localized IS does not show this rapid drop. Regardless of the initial conditions, the rate constants become similar to each other within 500 fs. As could be expected, $k_{\text{BPFMO}}(t)$ has no dependence on the initial state in the roll. It is, however, not easy to relate the time constants (τ_1 , τ_2 and τ_3) in Table I, which are usually reported for experimental data analysis [19, 22], to the time dependent rates in Fig. 8.

III. CONCLUSION

The green sulfur bacteria seems to be an incredibly efficient light processing machine (*cf.* purple bacterium in Ref. [92]): we showed this by investigating from all-atoms and a top to bottom approach. The excitation energy transfer route was taken from the chlorosome to the reaction center via the baseplate and FMO, under different initiating conditions. Analysis of the atomistic model indicates resonant energy transfer is maximized (faster) given the multichromophoric excitonic coupling which is due to the molecular arrangements of these parts: the green sulfur bacteria are assembled to be most conducive towards efficient excitation energy transfer within the Förster energy transfer regime. It was further shown that whether initial excitation is localized or delocalized (or a third scenario, in-between the two). Though, the results differ qualitatively within a short time limit (500 fs). None of these scenario's, however, adversely affect the efficiency of energy transfer and the results converge within the overall timescale (10 ps) [19, 22]. Thus the mechanism is robust to initial conditions, including varying temperatures (which seems necessary given green sulfur bacteria is thermophilic in nature). This due mainly to the fast internal exciton dynamics of the chlorosome, which is also observed in Refs. [71, 93]. Furthermore our measure of cooperativity quantifies this and indicates a preference (again regardless of initial conditions) to the polarization in the xy-plane (cross section of

the chlorosome), which enhances the excitonic coupling strengths between the exciton states of the chlorosome and the baseplate. We suggest a multichromophoric effect may prevail over the absence of proximity by exploiting the symmetry in parts of the model. This calculation of cooperativity indicates a supertransfer effect inherent in: the green sulfur bacteria, which seems to be especially “tuned” towards thriving under low light conditions by making use of molecular aggregates, symmetry and self-assembly to capture light and funnel it to the reaction center aided, not hindered, by a fluctuating environment [25, 94].

Additionally we would like to comment here on the role of the baseplate in the energy funneling process based on our simulations. In our model study, the baseplate plays the role of a “bridge” allowing the exciton energy to funnel down to the FMOs from the chlorosome. The presence of the baseplate eases this process; without the baseplate energy transfer would be impeded. Whilst it could be the case that transfer is allowed without the baseplate under the condition that the FMO's and chlorosomes be positioned close enough for Förster energy transfer our results indicates that the baseplate offers a preferred route. The baseplate receives the exciton quickly as shown in Fig. 4 and releases the exciton to the FMO complexes steadily. Since the chlorosome has a relatively large reorganization energy, which implies strong exciton-phonon couplings to the bath, compared to those of the baseplate and FMO complexes, the exciton could be lost to the environment if it is able to stay in the chlorosome for too long a time. Thus, we would like to introduce the idea of the baseplate as a biological “exciton capacitor”. It seems to be suitably designed for this purpose, making sure the route of the exciton is directed, by receiving the exciton from the chlorosome quickly, keeping the exciton from leaking to the surrounding environment, and supplying it to the FMO. It does so by providing appropriate excitonic sites, via chromophoric pigments, held in a unique and interestingly crystalline protein scaffold made of amphiphilic units that cross two very different dielectric boundaries (the interim gap between dry lipid chlorosomes and the more watery region at the FMOs) in a near perfect 2D lattice form in analogy to an actual capacitor (condenser) but made of soft materials.

Our model study depends on many undetermined parameters, such as the site energies of the baseplate, distance between the antenna units and the spectral density of the baseplate. However, our study shows characteristic time constants that fall within sub-100 fs-sub-100 ps and agree with experimental observations [19, 22] (or see Table I).

An even more fully comprehensive study using quantum mechanics/molecular mechanics (QM/MM) calculations for the whole system, including the reaction center, where the electron transfer occurs is in progress in our group.

ACKNOWLEDGMENTS

J. H. thanks Christoph Kreisbeck for the verification of numerical stability in the simulation and discussion about the spectral density. J. H., S. V., T. F. and A. A.-G. acknowledge support from the Center for Excitonics, an Energy Frontier Research Center funded by the

US Department of Energy, Office of Science and Office of Basic Energy Sciences under award DE-SC0001088. J. C. B. acknowledges support from Wellcome Trust UK. S. K. S. and A. A.-G. also acknowledge Defense Threat Reduction Agency grant HDTRA1-10-1-0046. Further, A. A.-G. is grateful for the support from Defense Advanced Research Projects Agency grant N66001-10-1-4063, and the Corning Foundation for their generous support.

-
- [1] R. E. Blankenship, *Molecular Mechanisms of Photosynthesis* (World Scientific, London, 2002).
- [2] G. T. Oostergetel, H. van Amerongen, and E. J. Boekema, *Photosynth. Res.* **104**, 245 (2010).
- [3] D. Canfield, B. Thamdrup, and E. Kristensen, *Aquatic geomicrobiology* (Elsevier, London, 2005).
- [4] J. Overmann, "The prokaryotes. volume 7: Proteobacteria: Delta, epsilon subclass," (Springer, 2006) Chap. The Family Chlorobiaceae, pp. 359–378.
- [5] X. Feng, K.-H. Tang, R. E. Blankenship, and Y. J. Tang, *J. Bio. Chem.* **285**, 39544 (2010).
- [6] J. Overmann, H. Cypionka, and N. Pfennig, *Limnol. Oceanog.* **37**, 150 (1992).
- [7] J. T. Beatty, J. Overmann, M. T. Lince, A. K. Manske, A. S. Lang, R. E. Blankenship, C. L. Van Dover, T. A. Martinson, and F. G. Plumley, *Proc. Natl. Acad. Sci.* **102**, 9306 (2005).
- [8] A. K. Manske, J. Glaeser, M. M. M. Kuypers, and J. Overmann, *Appl. Environ. Microbiol.* **71**, 8049 (2005).
- [9] G. Engel, T. Calhoun, E. Read, T. Ahn, T. Mancal, Y. Cheng, R. Blankenship, and G. Fleming, *Nature* **446**, 782 (2007).
- [10] G. D. Scholes, G. R. Fleming, A. Olaya-Castro, and R. van Grondelle, *Nat. Chem.* **3**, 763 (2011).
- [11] A. Borisov, *Biophysics* **57**, 562 (2012).
- [12] S. Lloyd and M. Mohseni, *New J. Phys.* **12**, 075020 (2010).
- [13] D. F. Abasto, M. Mohseni, S. Lloyd, and P. Zanardi, *Phil. Trans. R. Soc. A* **370**, 3750 (2013).
- [14] I. Kassal, J. Yuen-Zhou, and S. Rahimi-Keshari, *J. Phys. Chem. Lett.* **4**, 362 (2013).
- [15] S. Savikhin, P. I. van Noort, Y. Zhu, S. Lin, R. E. Blankenship, and W. S. Struve, *Chem. Phys.* **194**, 245 (1995).
- [16] J. Psencik, T. Polívka, J. Dian, J. Kudrna, and P. Malý, *J. Phys. Chem. A* **102**, 4392 (1998).
- [17] V. I. Prokhorenko, D. B. Steensgaard, and A. R. Holzwarth, *Biophys. J.* **79**, 2105 (2000).
- [18] J. Psencik, Y.-Z. Ma, J. B. Arellano, J. Hála, and T. Gillbro, *Biophys. J.* **84**, 1161 (2003).
- [19] J. Martiskainen, J. Linnanto, V. Aumanen, P. Myllyperkiö, and J. Korppi-Tommola, *Photochem. Photobiol.* **88**, 675 (2012).
- [20] Z. Fetisova, a. Freiberg, K. Mairing, V. Novoderezhkin, a. Taisova, and K. Timpmann, *Biophys. J.* **71**, 995 (1996).
- [21] Y. Shibata, Y. Saga, H. Tamiaki, and S. Itoh, *Biochemistry* **46**, 7062 (2007).
- [22] J. Martiskainen, J. Linnanto, R. Kananavičius, V. Lehtovuori, and J. Korppi-Tommola, *Chem. Phys. Lett.* **477**, 216 (2009).
- [23] K. Mukai, S. Abe, and H. Sumi, *J. Phys. Chem. B* **103**, 6096 (1999).
- [24] S. Jang, M. D. Newton, and R. J. Silbey, *J. Phys. Chem. B* **111**, 6807 (2007).
- [25] M. Mohseni, P. Rebertrost, S. Lloyd, and A. Aspuru-Guzik, *J. Chem. Phys.* **129**, 174106 (2008).
- [26] A. Ishizaki and G. R. Fleming, *Proc. Natl. Acad. Sci.* **106**, 17255 (2009).
- [27] J. Strümpfer and K. Schulten, *J. Chem. Phys.* **131**, 225101 (2009).
- [28] G. Ritschel, J. Roden, W. T. Strunz, A. Aspuru-Guzik, and A. Eisfeld, *J. Phys. Chem. Lett.* **2**, 2912 (2011).
- [29] S. Shim, P. Rebertrost, S. Valteau, and A. Aspuru-Guzik, *Biophys. J.* **102**, 649 (2012).
- [30] C. Kreisbeck and T. Kramer, *J. Phys. Chem. Lett.* **3**, 2828 (2012).
- [31] H. W. Kim, A. Kelly, J. W. Park, and Y. M. Rhee, *J. Am. Chem. Soc.* **134**, 11640 (2012).
- [32] A. Damjanović, I. Kosztin, U. Kleinekathöfer, and K. Schulten, *Phys. Rev. E* **65**, 1 (2002).
- [33] C. Olbrich and U. Kleinekathöfer, *J. Phys. Chem. B* **114**, 12427 (2010).
- [34] X. Hu, T. Ritz, A. Damjanovic, and K. Schulten, *J. Phys. Chem. B* **101**, 3854 (1997).
- [35] M. K. Sener, J. D. Olsen, C. N. Hunter, and K. Schulten, *Proc. Natl. Acad. Sci.* **104**, 15723 (2007).
- [36] A. Olaya-Castro, C. Lee, F. Olsen, and N. Johnson, *Phys. Rev. B* **78**, 085115 (2008).
- [37] A. K. Ringsmuth, G. J. Milburn, and T. M. Stace, *Nat. Phys.* **8**, 562 (2012).
- [38] J. Dostál, T. Mančal, R. Augulis, F. Vácha, J. Pšenčík, and D. Zigmantas, *J. Am. Chem. Soc.* **134**, 11611 (2012).
- [39] J. Cao and R. J. Silbey, *J. Phys. Chem. A* **113**, 13825 (2009).
- [40] F. Caruso, A. W. Chin, A. Datta, S. F. Huelga, and M. B. Plenio, *J. Chem. Phys.* **131**, 105106 (2009).
- [41] M. O. Pedersen, J. Linnanto, N.-U. Frigaard, N. C. Nielsen, and M. Miller, *Photosynth. Res.* **104**, 233 (2010).
- [42] J. M. Olson, *Photosynth. Res.* **80**, 181 (2004).
- [43] T. Förster, *Ann. Phys.* **437**, 55 (1948).
- [44] V. May and O. Kühn, *Charge and Energy Transfer Dynamics in Molecular Systems*, 3rd ed. (Wiley-VCH, New York, 2011).
- [45] E. N. Zimanyi and R. J. Silbey, *Phil. Trans. R. Soc. A* **370**, 3620 (2012).
- [46] N.-U. Frigaard, A. G. M. Chew, H. Li, J. A. Maresca, and D. A. Bryant, *Photosynth. Res.* **78**, 93 (2003).
- [47] J. M. Linnanto and J. E. I. Korppi-Tommola, *Photosynth. Res.* **96**, 227 (2008).
- [48] S. Ganapathy, G. T. Oostergetel, P. K. Wawrzyniak,

- M. Reus, A. Gomez Maqueo Chew, F. Buda, E. J. Boekema, D. A. Bryant, A. R. Holzwarth, and H. J. M. de Groot, *Proc. Natl. Acad. Sci.* **106**, 8525 (2009).
- [49] Y. Tian, R. Camacho, D. Thomsson, M. Reus, A. R. Holzwarth, and I. G. Scheblykin, *J. Am. Chem. Soc.* **133**, 17192 (2011).
- [50] M. O. S. Pedersen, J. Underhaug, J. Dittmer, M. Miller, and N. C. Nielsen, *FEBS letters* **582**, 2869 (2008).
- [51] J. Phillips, R. Braun, W. Wang, J. Gumbart, E. Tajkhorshid, E. Villa, C. Chipot, R. Skeel, L. Kale, and K. Schulten, *J. Comput. Chem.* **26**, 1781 (2005).
- [52] V. Hornak, R. Abel, A. Okur, B. Strockbine, A. Roitberg, and C. Simmerling, *Proteins* **65**, 712 (2006).
- [53] R. E. Blankenship, M. T. Madigan, and C. E. Bauer, *Anoxygenic photosynthetic bacteria* (Kluwer Academic Publishers, New York, 1995).
- [54] D. E. Tronrud, J. Wen, L. Gay, and R. E. Blankenship, *Photosynth. Res.* **100**, 79 (2009).
- [55] J. Wen, H. Zhang, M. L. Gross, and R. E. Blankenship, *Proc. Natl. Acad. Sci.* **106**, 6134 (2009).
- [56] M. Schmidt am Busch, F. Müh, M. El-Amine Madjet, and T. Renger, *J. Phys. Chem. Lett.* **2**, 93 (2011).
- [57] J. Adolphs and T. Renger, *Biophys. J.* **91**, 2778 (2006).
- [58] M. T. W. Milder, B. Brüggemann, R. van Grondelle, and J. L. Herek, *Photosynth. Res.* **104**, 257 (2010).
- [59] C. Francke and J. Ames, *Photosynth. Res.* , 137 (1997).
- [60] V. I. Prokhorenko, D. B. Steensgaard, and A. R. Holzwarth, *Biophys. J.* **85**, 3173 (2003).
- [61] W. H. Louisell, *Quantum Statistical Properties of Radiation* (John Wiley & Sons, New York, 1973).
- [62] H. P. Breuer and F. Petruccione, *The Theory of Open Quantum Systems* (Oxford University, Oxford, 2006).
- [63] P. Rebentrost, R. Chakraborty, and A. Aspuru-Guzik, *J. Chem. Phys.* **131**, 184102 (2009).
- [64] P. Rebentrost, M. Mohseni, and A. Aspuru-Guzik, *J. Phys. Chem. B* **113**, 9942 (2009).
- [65] W. M. Zhang, T. Meier, V. Chernyak, and S. Mukamel, *J. Chem. Phys.* **108**, 7763 (1998).
- [66] T. Pullerits, *J. Chin. Chem. Soc.* **47**, 773 (2000).
- [67] M. Yang and G. R. Fleming, *Chem. Phys.* **275**, 355 (2002).
- [68] V. Novoderezhkin, J. M. Salverda, and H. V. Amerongen, *J. Phys. Chem. B* , 1893 (2003).
- [69] V. I. Novoderezhkin, M. A. Palacios, and H. V. Amerongen, *J. Phys. Chem. B* , 10363 (2004).
- [70] A. Ishizaki and G. R. Fleming, *J. Chem. Phys.* **130**, 234110 (2009).
- [71] T. Fujita, J. C. Brookes, S. K. Saikin, and A. Aspuru-Guzik, *J. Phys. Chem. Lett.* **3**, 2357 (2012).
- [72] A. Ishizaki and G. R. Fleming, *J. Chem. Phys.* **130**, 234111 (2009).
- [73] C. Kreisbeck, T. Kramer, M. Rodríguez, and B. Hein, *J. Chem. Theory Comput.* **7**, 2166 (2011).
- [74] J. Zhu, S. Kais, P. Rebentrost, and A. Aspuru-Guzik, *J. Phys. Chem. B* **115**, 1531 (2011).
- [75] P. Huo and D. F. Coker, *J. Phys. Chem. Lett.* **2**, 825 (2011).
- [76] G. Ritschel, J. Roden, W. T. Strunz, and A. Eisfeld, *New J. Phys.* **13**, 113034 (2011).
- [77] D. P. S. Mccutcheon and A. Nazir, *J. Chem. Phys.* **135**, 114501 (2011).
- [78] L. Mühlbacher and U. Kleinekathöfer, *J. Phys. Chem. B* **116**, 3900 (2012).
- [79] L. A. Pachón and P. Brumer, *Phys. Chem. Chem. Phys.* **14**, 10094 (2012).
- [80] Y. Kubota and K. Nobusada, *J. Chem. Phys.* **129**, 094704 (2003).
- [81] I. Kondov, U. Kleinekathöfer, and M. Schreiber, *J. Chem. Phys.* **119**, 6635 (2003), arXiv:0307050 [physics].
- [82] S. Valteau, A. Eisfeld, and A. Aspuru-Guzik, *J. Chem. Phys.* **137**, 224103 (2012).
- [83] S. Geiger, G. Lord, and A. Tambue, *Comput. Geosci.* **16**, 323 (2012).
- [84] S. Savikhin, D. R. Buck, and W. S. Struve, *Biophys. J.* **73**, 2090 (1997).
- [85] P. Brumer and M. Shapiro, *Proc. Natl. Acad. Sci.* **109**, 19575 (2012).
- [86] S. Jang, M. Newton, and R. Silbey, *Phys. Rev. Lett.* **92**, 218301 (2004).
- [87] J. Roden, G. Schulz, A. Eisfeld, and J. Briggs, *J. Chem. Phys.* **131**, 044909 (2009).
- [88] T. P. Causgrove, D. C. Brune, and R. E. Blankenship, *J. Photochem. Photobiol. B: Biol.* **15**, 171 (1992).
- [89] J. Strümpfer, M. Sener, and K. Schulten, *J. Phys. Chem. Lett.* **3**, 536 (2012).
- [90] M. Yang and G. R. Fleming, *J. Chem. Phys.* **119**, 5614 (2003).
- [91] L. Valkunas, J. Chmeliov, G. Trinkunas, C. D. P. Duffy, R. van Grondelle, and A. V. Ruban, *J. Phys. Chem. B* **115**, 9252 (2011).
- [92] R. Hildner, D. Brinks, J. B. Nieder, R. J. Cogdell, and N. F. van Hulst, *Science* **340**, 1448 (2013).
- [93] T. Fujita, J. Huh, S. K. Saikin, J. C. Brookes, and A. Aspuru-Guzik, arXiv:1304.4902v2 (2013), arXiv:1304.4902.
- [94] P. Rebentrost, M. Mohseni, I. Kassal, S. Lloyd, and A. Aspuru-Guzik, *New J. Phys.* **11**, 033003 (2009).